A DFT-Based QM-MM Approach Designed for the Treatment of Large Molecular Systems: Application to Chorismate Mutase

Alejandro Crespo,[†,§] Damián A. Scherlis,[†,‡] Marcelo A. Martí,[†] Pablo Ordejón,[‡] Adrián E. Roitberg,[*,§] and Darío A. Estrin[*,†]

Departamento de Química Inorgánica, Analítica y Química-Física and INQUIMAE-CONICET, Facultad de Ciencias Exactas y Naturales, Universidad de Buenos Aires, Ciudad Universitaria - Pab II, C1428EHA Buenos Aires, Argentina, Institut de Ciencia de Materials de Barcelona−CSIC, Campus de la U.A.B., 08193 Bellaterra, Barcelona, Spain, and Quantum Theory Project and Department of Chemistry, University of Florida, Gainesville, Florida 32611-8435

Received: July 30, 2003; In Final Form: October 6, 2003

We present a density functional theory (DFT) hybrid quantum mechanical/molecular mechanical (QM-MM) implementation developed for simulations of reactions in complex environments. It is particularly suited to study enzyme active sites or solutes in condensed phases. The method combines a QM description of the solute with a MM treatment of the environment. The QM fragment is treated using DFT as implemented in the computationally efficient program SIESTA, while the environment is treated using the Wang et al. Amber force field parametrization. We applied our new QM-MM scheme to study the conversion of chorismate to prephenate by computing the reaction energy profile in vacuo, aqueous solution and in the active site of the *B. subtilis* chorismate mutase enzyme. We have performed calculations for two different choices of the QM subsystem in the enzyme simulations: including only the substrate moiety and the substrate plus the charged side chains glu78 and arg90, respectively. In both cases, our results are in good agreement with experiment. The catalytic activity achieved by chorismate mutase relative to the uncatalyzed reaction in solution is due to both a minor destabilization of the substrate molecule by compression and a major electrostatic stabilization of the transition state, which reduce the activation energy of the reaction.

Introduction

Computer simulation has drastically changed chemists' perception and understanding of chemical reactivity. Progress in the area of accurate quantum chemical treatments of isolated molecules has been impressive. However, the goal of describing chemical processes in complex environments such as solvated biomolecules at the same level of accuracy has not been achieved yet, and the development and validation of theoretical models which balance accuracy and computational efficiency is a very active research area. Due to the nonlinear increase of computational cost of quantum mechanical (QM) calculations, the treatment of very large systems at the QM level is not presently feasible. One way to overcome this limitation has been oriented to the development of linear-scaling electronic structure methods.[1−6] An alternative strategy is to employ hybrid quantum mechanical/molecular mechanical (QM-MM) schemes. These schemes are adequate for the investigation of chemical events that take place in a certain region of a large system, which is modeled using QM (QM region), while the remainder of the system (MM region) is treated at the less expensive MM level. The use of these kinds of techniques for the investigation of chemical reactivity in solution and in enzymes has increased enormously in the past years.[7−13]

Due to the fact that a large degree of configurational sampling is necessary in most biological applications, the computational expense of QM-MM implementations remains a crucial issue, and the electronic structure scheme should be carefully chosen in order to provide accurate results at low cost for each particular problem. The use of QM-MM schemes in which the QM calculation involves a linear scaling approach may be the best strategy for dealing with problems in which it is necessary to select a large QM subsystem. In this work we present a QM-MM method to treat biological macromolecules in complex environments. Our scheme uses, for the description of the QM region, a very efficient implementation of density functional theory (DFT) based on numerical basis sets called SIESTA (Spanish Initiative for Electronic Simulation of Thousands of Atoms).[14,15] The classical subsystem is treated using the Wang et al. Amber force field parametrization, containing stretching, bending, and torsional terms, atom-centered charges, and Lennard−Jones potential interactions.[16]

To present our QM-MM scheme, we have examined the reaction path of the conversion of chorismate to prephenate (Scheme 1), a problem for which there is an important body of theoretical and experimental data. This intramolecular transformation is of special interest because it proceeds both uncatalyzed in water solution and catalyzed by the enzyme chorismate mutase, providing a unique opportunity to compare the catalyzed and uncatalyzed reactions.[17] Chorismate mutase is an essential enzyme in the Shikimate pathway. This pathway is responsible for the biosynthesis of aromatic amino acids in bacteria, fungi, and plants, but not in mammals.[18] The enzyme is of interest not only for an understanding of its catalytic rate enhancement, but also as a target for the discovery of antibiotics, antifungals, and herbicides. For these reasons, chorismate mutase

* Corresponding authors. E-mail: roitberg@qtp.ufl.edu; dario@qi.fcen.uba.ar
† Universidad de Buenos Aires.
‡ Institut de Ciencia de Materials de Barcelona.
§ University of Florida.

10.1021/jp036236h CCC: $25.00
Published on Web 11/15/2003

SCHEME 1. Chorismate Conformational Preequilibrium (left) and Conversion to Prephenate (right)

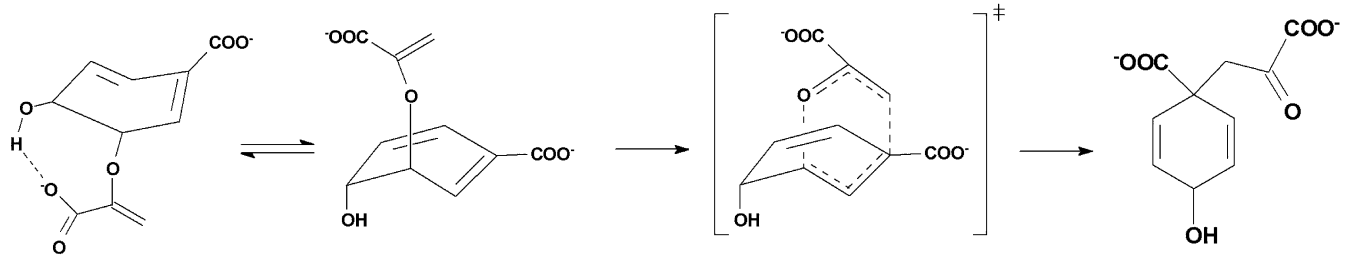

Diequatorial Chorismate Diaxial Chorismate Transition State Prephenate

has been the focus of numerous studies in the past decades.[19−35] Our calculations provide a clear improvement with respect to previous AM1[26,27,33,34] and HF-based calculations,[30] which may present flaws in the description of transition states and overestimate the activation energy.

The experimental activation parameters for the uncatalyzed reaction of chorismate to form prephenate in aqueous solution at pH 7.5 are $\Delta H^{\ddagger} = 20.7$ kcal/mol and $\Delta S^{\ddagger} = -12.9$ eu.[19] The enzyme chorismate mutase accelerates the reaction by a factor of about 10^6 over the uncatalyzed reaction. The activation parameters for the *B. subtilis* chorismate mutase reported by Kast et al.[20] are $\Delta H^{\ddagger} = 12.7$ kcal/mol and $\Delta S^{\ddagger} = -9.1$ eu. They concluded that lowering the entropy barrier of the reaction is not a major factor in catalysis in *B. subtilis* chorismate mutase, because $\Delta S^{\ddagger}$ in this case is unfavorable and comparable to that for the uncatalyzed reaction.

Chorismate has been found to adopt several conformations in vacuum and in condensed phase. The more populated conformations in vacuum are the pseudodiequatorial and pseudodiaxial, with the pseudodiequatorial being the most stable.[20,21,23,27] The rearrangement of chorismate to prephenate requires a conformational change in which the diequatorial conformer is converted to the diaxial one, which is the reactive conformer capable of progressing via the pericyclic rearrangement to prephenate (Scheme 1) with a chair-like transition state. Several researchers have applied theoretical methods to study the conformational preequilibrium of chorismate. One of the first theoretical works was done by Wiest and Houk, who located and characterized as minima two chorismate conformers at the Hartree−Fock and density functional theory level (RHF/6-31G* and BLYP/6-31G*, respectively).[21,23] The mechanism of chorismate mutase has been studied by Khanjin et al. by performing B3LYP/6-31G* calculations on several chorismate conformationally restricted analogues.[25] Marti et al.[27] found five chorismate conformers as minima in vacuum. Hillier and co-workers[24] examined the effect of water on the conformational energetics of chorismate conformers by both a polarized continuum model (PCM) and explicit solvation within a Monte Carlo free energy perturbation (MC/FEP) treatment, and concluded that solvation reduces the energy difference between the diequatorial and diaxial structures, but still the diequatorial form was the most stable. Guo et al.[35] found two nonreactive conformers that are more stable than the reactive diaxial conformer in solution and which resemble the diequatorial conformers, using B3LYP/6-31G* and PCM. However, they showed that these conformers rapidly convert (approximately in 5 ps) to the active diaxial conformer in the active site of chorismate mutase using self-consistent charge density functional tight-binding (SCC-DFTB) calculations.

More recently, Jorgensen and co-workers, studied the environment effects of the reaction in water and in the active site of chorismate mutase. They used a combined QM-MM MC/FEP method and applied the concept of near attack conformations (NACs) to chorismate.[33,34] They showed that 1%, 82%, and 100% of chorismate conformers were found to be NACs structures, or active conformers, in vacuum, water, and in the enzyme, respectively. Moreover, they calculated the activation free energy of the conformational preequilibrium of chorismate, showing that only in the gas phase does this step provide a positive contribution to the total activation free energy of the reaction (approximately 3, −1, and −9 kcal/mol in a vacuum, water and enzyme, respectively). They proposed that the rate enhancement by chorismate mutase over the uncatalyzed aqueous reaction results primarily from conformational compression of the reactant by the enzyme and suggested that the preferential stabilization of the transition state in the enzyme environment relative to water played a secondary role.[34] On the other hand, Marti et al.[26] calculated the free energy profile for the reaction in aqueous solution and in the enzyme, and concluded that the enzyme preferentially binds the reactive diaxial conformer of chorismate, and it reduces the activation free energy of the reaction relative to that in solution by providing an environment which preferentially stabilizes the transition state. Lee et al.[30] assessed the role of different residues in the stabilization of the transition state by performing QM-MM calculations at the HF level. Recently, a QM-MM pathway optimization study of the conversion of chorismate to prephenate performed using a combination of HF/4-31G and B3LYP/6-31G** electronic structure methods has been reported.[31] Most of these QM-MM calculations were performed using HF[30] or AM1 Hamiltonians.[26,27,33,34] For this reason, it is interesting to reanalyze the subject using a more accurate electronic structure DFT scheme.

The main objectives of this work are to present a QM-MM method which uses a very efficient implementation of DFT called SIESTA, and to test it in the conversion of chorismate to prephenate. We have employed a restrained energy minimization scheme to obtain the reaction energy profiles in vacuum, aqueous solution, and in the enzyme environment. Entropic contributions are much more difficult to asses and are neglected in the present work since, according to experimental results, they play a minor role in the catalysis.[20] If needed, they would have to be included by sampling the degrees of freedom orthogonal to the reaction coordinate by performing molecular dynamics simulations. We will shed light on the enzymatic mechanism, particularly to understand if the catalytic activity is due to a conformational compression of the reactant, a preferential stabilization of the transition state, or both. To

SCHEME 2. QM Subsystem Model of the Reactant with Its Relevant Numbering

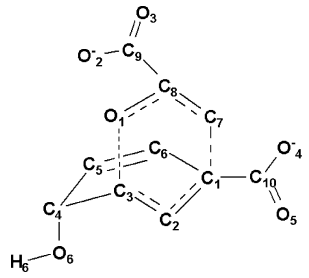

SCHEME 3. QM Subsystem Model Including the Reactant Plus the Charged Side Chains Glu78 and Arg90

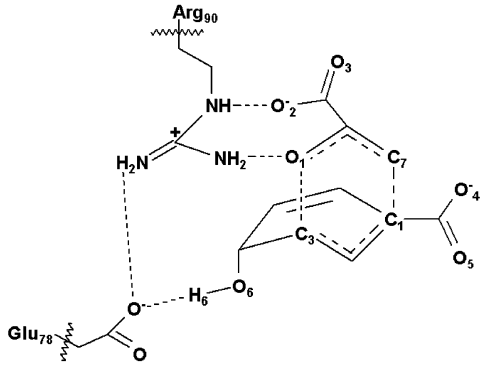

consider charge transfer to the substrate and polarization effects in neighbor charged residues, we have performed calculations for two different choices of the QM subsystem, one including only the substrate moiety (Scheme 2) and another with the substrate plus the charged side chains glu78 and arg90 (Scheme 3).

QM-MM Implementation Details

A. The SIESTA Electronic Structure Method. An extensive review on the technicalities and the performance of the SIESTA program can be found in previous works.[14,36,37] A remarkable feature of SIESTA is the use of flexible basis sets consisting of linear combinations of finite atomic orbitals defined in a real space grid. The program has been optimized to yield order *N* scaling for large systems. Moreover, the program is extremely fast and efficient in comparison with conventional Gaussian or plane waves schemes for medium size species. The algorithms perform all the required calculations numerically, so that basis functions are not constrained to any analytical functional form, and the matching of the radial wave function to the core region, described by pseudopotentials, is inexpensive. In particular, it was found to be convenient to implement the so-called pseudo atomic orbitals (PAOs), which are the eigenfunctions of the atomic pseudopotential problem confined in an infinite potential sphere.[38] The confinement originates finite range PAOs with higher kinetic energies than the free eigenfunctions. By keeping this increment in the energy at the same amount for all the PAOs, the basis is obtained in a balanced way. Split valence bases may be generated by combining suitable Gaussian (numerical) orbitals on top of the minimal basis described above.

The nuclei and inner electrons are represented by norm-conserving pseudopotentials to avoid the computation of core states, smoothing at the same time the valence charge density and therefore relaxing the quality requirements on the grid. Within the nonlocal pseudopotential approximation, the Kohn−Sham Hamiltonian may be written

$$H = T + \sum_{\alpha} [V_{\alpha}^{\text{local}} + V_{\alpha}^{\text{nl}}] + V^{\text{H}}(\mathbf{r}) + V^{\text{xc}}(\mathbf{r}) \qquad (1)$$

where α is an atom index, T is the kinetic energy operator, and V^{H} and V^{xc} are the Hartree and exchange-correlation potentials, respectively. The pseudopotential is split into two contributions: a local part $V_{\alpha}^{\text{local}}$ independent of the angular momentum *lm* of the core electrons, determining the long-range interaction;, and a nonlocal part V_{α}^{nl} that operates selectively on the valence electrons.

$$\hat{V}_{\alpha}^{\text{nl}} = \sum_{lm} |\phi_{\alpha lm}^{\text{KB}}\rangle \epsilon_{\alpha l}^{\text{KB}} \langle \phi_{\alpha lm}^{\text{KB}}| \qquad (2)$$

with

$$\phi_{\alpha lm}^{\text{KB}}(\mathbf{r}) = [V_{\alpha l}(\mathbf{r}) - V_{\alpha}^{\text{local}}(\mathbf{r})]\, \psi_{\alpha lm}(\mathbf{r}) \qquad (3)$$

$$\epsilon_{\alpha l}^{\text{KB}} = \langle \psi_{\alpha lm}|\, V_{\alpha l} - V_{\alpha}^{\text{local}} |\psi_{\alpha lm}\rangle^{-1} \qquad (4)$$

where $\psi_{\alpha lm}$ are the atomic pseudoorbitals, for instance the eigenfunctions of the radial potentials $V_{\alpha l}(\mathbf{r})$. The terms $\phi_{\alpha lm}^{\text{KB}}$ are known as the Kleinman−Bylander projectors.[39] Note that since $V_{\alpha l}(\mathbf{r}) - V_{\alpha}^{\text{local}}(\mathbf{r})$ is nonzero only inside a small radius, V_{α}^{nl} will be zero beyond this radius, as expected for a short-range operator.

If we call $\rho_{\alpha}^{\text{atom}}$ the charge density of the isolated atoms and $\rho^{\text{na}}(\mathbf{r}) = \Sigma_{\alpha}\rho_{\alpha}^{\text{atom}}(|\mathbf{r} - \mathbf{r}_{\alpha}|)$, then it is possible to define $\delta\rho(\mathbf{r}) = \rho(\mathbf{r}) - \rho^{\text{na}}(\mathbf{r})$ as the difference between the self-consistent and the nonperturbed electronic density. $\delta\rho(\mathbf{r})$ represents a small value against $\rho(\mathbf{r})$, increasing the precision of numerical integrals and allowing to rewrite the Hamiltonian in the following way:

$$H = T + \sum_{\alpha} V_{\alpha}^{\text{nl}} + \sum_{\alpha} V_{\alpha}^{\text{na}}(\mathbf{r}) + \delta V^{\text{H}}(\mathbf{r}) + V^{\text{xc}}(\mathbf{r}) \qquad (5)$$

with δV^{H} the potential associated to $\delta\rho$. The long range of $V_{\alpha}^{\text{local}}$ is eliminated by screening it with V_{α}^{atom}, created by the atomic electron density $\rho_{\alpha}^{\text{atom}}$, to produce a short range "neutral atom" potential $V_{\alpha}^{\text{na}} \equiv V_{\alpha}^{\text{local}} + V_{\alpha}^{\text{atom}}$. Matrix elements corresponding to the two former terms on the right side in the eq 5 involve two center integrals evaluated once in reciprocal space at the beginning of the iterative process. The other terms are obtained by numerical integration in real space. In this context, the expression for the Kohn−Sham energy may be written as

$$E_{\text{KS}} = \sum_{\mu\nu} P_{\mu\nu} H_{\mu\nu} - \frac{1}{2}\int V^{\text{H}}(\mathbf{r})\, \rho(\mathbf{r})\, \mathrm{d}\mathbf{r} + \int (\epsilon^{\text{xc}}(\mathbf{r}) - V^{\text{xc}}(\mathbf{r}))\, \rho(\mathbf{r})\, \mathrm{d}\mathbf{r} + \frac{1}{2}\sum_{\alpha\beta} \frac{Z_{\alpha} Z_{\beta}}{r_{\alpha\beta}} \qquad (6)$$

where $P_{\mu\nu}$ and $H_{\mu\nu}$ are the density and the Hamiltonian matrix elements, Z_{α} the charge of the core, and $\epsilon^{\text{xc}}(\mathbf{r})\rho(\mathbf{r})$ the exchange-correlation energy density. In particular, the Hartree potential $\delta V^{\text{H}}(\mathbf{r})$ is calculated from the self-consistent $\delta\rho(\mathbf{r})$ by inverting the Poisson equation in the reciprocal space using the standard fast Fourier transform method. The self-consistent potential is thus obtained as a numerical function in real space, avoiding the cost of evaluating the two electrons and four center integrals usually associated with the Coulombic terms. Since the potential and the electronic density are transformed back and forth

between the real and the reciprocal space, they are periodic functions suitable for the treatment of solids and extended phases. Simulations in molecular systems may be performed as well, providing the size of the grid is large enough to avoid self-interaction effects.

All calculations have been performed using DZVP basis sets, with a pseudoatomic orbital energy shift of 30 meV, a grid cutoff of 150 Ry,[14,36,37] and the generalized gradient approximation of Perdew, Burke, and Ernzerhof.[40]

B. Molecular Mechanics Model. In our scheme the solvent or the environment is represented by an appropriate classical potential. For the treatment of biological macromolecular environments, we implemented the Wang et al. force field parametrization,[16] which describes the intramolecular energy by setting force constants for bonds, angles, and torsions, and also electrostatic and van der Waals interactions for those pairs separated by at least three bonds:

$$E_{\mathrm{MM}} = \sum_{\text{bonds}} K_{\mathrm{b}}(b - b_{\mathrm{eq}})^2 + \sum_{\text{angles}} K_{\theta}(\theta - \theta_{\mathrm{eq}})^2 + \sum_{\text{dihedrals}} \frac{V_n}{2}[1 + \cos(n\phi - \gamma)] + \sum_{i,j}\left[\frac{A_{ij}}{R_{ij}^{12}} - \frac{B_{ij}}{R_{ij}^{6}} + \frac{q_i q_j}{R_{ij}}\right] \quad (7)$$

The TIP3P model is employed to describe water molecules.[41]

C. The QM-MM Scheme. The quantum and the molecular mechanics calculations are combined through a hybrid Hamiltonian H_{TOT} introducing a coupling term, $H_{\mathrm{QM-MM}}$:

$$H_{\mathrm{TOT}} = H_{\mathrm{QM}} + H_{\mathrm{MM}} + H_{\mathrm{QM-MM}} \quad (8)$$

with

$$E_{\mathrm{TOT}} = E_{\mathrm{KS}} + E_{\mathrm{MM}} + E_{\mathrm{QM-MM}} \quad (9)$$

Here E_{KS} is the Kohn−Sham energy of eq 6 and E_{MM} is the molecular mechanics energy defined in eq 7, whereas the hybrid term $E_{\mathrm{QM-MM}}$ may be decomposed into three contributions:

$$E_{\mathrm{QM-MM}} = \sum_{i=1}^{C} q_i \int \frac{\rho(\mathbf{r})}{|\mathbf{r} - \tau_i|}\,\mathrm{d}\mathbf{r} + \sum_{i=1}^{C}\sum_{\alpha=1}^{A} \frac{q_i Z_\alpha}{|\mathbf{R}_\alpha - \tau_i|} + E^{\mathrm{LJ}} \quad (10)$$

Here C is the number of atoms in the classical region, whose charges q_i are determined by the force field chosen to model the environment and α is an index on the A nuclei inside the quantum subsystem with core charges Z_α. The first term on the right in eq 10 represents the electrostatic interaction between the electrons and the classical charges and is obtained by numerical integration over the grid. The next term stands for the electrostatic interactions between the nuclei in the quantum subsystem and the classical point charges. Finally, E^{LJ} models the van der Waals interactions between the atoms in the quantum and classical regions through a 6−12 Lennard-Jones potential. The Lennard-Jones parameters for the QM atoms have been taken from the Wang et al. force field parametrization,[16] and have also been applied to chorismate in an earlier work.[32] The parameters have been tested by performing QM-MM calculations in selected chorismate (QM) − water (MM) dimers. Results for hydrogen bond distances and interaction energies were in good agreement with full QM calculations.

The environmet affects the charge density in a self-consistent fashion by the addition of the point charge potential to the Hartree potential δV^{H}.

$$\delta V^{\mathrm{H}}(\mathbf{r}) = \delta V^{\mathrm{H}}(\mathbf{r}) + \sum_{i=1}^{C} V_i^{\mathrm{MM}}(\mathbf{r}) \quad (11)$$

$$V_i^{\mathrm{MM}}(\mathbf{r}) = \frac{q_i}{|\tau_i - \mathbf{r}|} \quad (12)$$

Since the potential is evaluated numerically, the computational expense associated with this sum is proportional to C times the number of elements in the grid. Because of this, the incorporation of a classical potential is more expensive than in the case of a Gaussian scheme, where the integrals are performed analytically.[13] Still, the cost of the numerical QM-MM algorithm remains relatively small in comparison with the Kohn−Sham diagonalization procedure. The sum given in eq 11 is performed at every iteration in a step preceding the calculation of the Hamiltonian and other potential-dependent matrix elements, hence introducing the effect of the external classical potential in the electronic wave function and in the forces in a direct way. Forces on the QM nuclei are obtained by differentiation of eq 6 with respect to atomic positions, plus the derivative of the coupling energy $E_{\mathrm{QM-MM}}$.

$$\boldsymbol{F}_\alpha = -\frac{\partial E_{\mathrm{KS}}[\mathbf{R}]}{\partial \mathbf{R}_\alpha} - \frac{\partial E_{\mathrm{QM-MM}}[\mathbf{R},\tau]}{\partial \mathbf{R}_\alpha} \quad (13)$$

E_{KS} depends only on the molecular mechanics subsystem through $V^{\mathrm{H}}(\mathbf{r})$, contained in the second term on the right in eq 6. It can be shown[37] that the differentiation of $\int V^{\mathrm{H}}(\mathbf{r})\rho(\mathbf{r})\,\mathrm{d}\mathbf{r}$ ultimately leads to an expression whose overall dependence on $V^{\mathrm{H}}(\mathbf{r})$ is through a term of the form $Re\Sigma_\mu\Sigma_{\nu\in\alpha}P_{\mu\nu}\langle\phi_\mu|V^{\mathrm{H}}(\mathbf{r})|\nabla\phi_\nu\rangle$, meaning that the action of the MM potential on the forces is implicitly included if the contribution of $V^{\mathrm{MM}}(\mathbf{r})$ is previously added. Regarding the contribution of $E_{\mathrm{QM-MM}}$, the first term in eq 11 vanishes upon differentiation with respect to the QM atomic coordinates, while the other two have analytical derivatives. On the other hand, forces on the MM atoms are computed as the derivative of E_{MM} and $E_{\mathrm{QM-MM}}$ with respect to the classical atomic positions:

$$\mathbf{F}_i = -\frac{\partial E_{\mathrm{MM}}[\tau]}{\partial \tau_i} - \frac{\partial E_{\mathrm{QM-MM}}[\mathbf{R},\tau]}{\partial \tau_i} \quad (14)$$

The first term on the right in the equation above, as well as two of the three terms involved in $\partial E_{\mathrm{QM-MM}}/\partial\tau_i$, have analytical expressions. The only term that needs to be evaluated numerically is $\partial/\partial\tau_i \int\rho(\mathbf{r})\,|\mathbf{r} - \tau_i|^{-1}\,\mathrm{d}\mathbf{r}$, which is done together with the calculation of $E_{\mathrm{QM-MM}}$ after self-consistency is achieved.

The potential due to the classical charges, while proportional to the inverse of the distance, may become too steep at certain points inside the grid, affecting the numerical integrations. To preserve the smoothness of $\delta V^{\mathrm{H}}(\mathbf{r})$, the classical potential is truncated at short distances so that

$$V_i^{\mathrm{MM}}(\mathbf{r}) = \frac{q_i}{|\tau_i - \mathbf{r}|} \quad |\tau_i - \mathbf{r}| > R_{\mathrm{c}}$$

$$V_i^{\mathrm{MM}}(\mathbf{r}) = \frac{q_i}{R_c} \quad |\tau_i - \mathbf{r}| \le R_{\mathrm{c}}$$

It has been found that a value of R_{c} close to 0.2 or 0.3 Å is enough to avoid numerical problems without significantly affecting geometries or energies.

TABLE 1: Selected Geometrical Parameters of Chorismate Diequatorial Conformer and Prephenate in Vacuum (Å and degrees)[a]

	chorismate		prephenate	
	PBE/DZVP	B3LYP/6-31G**	PBE/DZVP	B3LYP/6-31G**
C1−C7	4.42	4.41	1.58	1.58
C3−C1	1.45	1.45	3.83	3.80
O2−H6	1.57	1.68	4.74	4.62
C3−O1−C8	119.1	121.2		
C1−C7−C8			116.5	116.2
O2−C9−C8−C7	163.7	153.2	117.0	121.7

[a] The PBE/DZVP and B3LYP/6-31G** calculations were performed using SIESTA and *Gaussian*98, respectively.

Notice that the point charges may be placed as far from the QM region as desired, regardless of the boundaries of the box. In fact, whether the MM atoms are inside or outside the box does not make any difference in terms of computational effort, neither if they are scattered along a large region in space. This is not true for the QM part, which size actually determines the size of the grid and therefore the cost of the numerical integrals.

D. Reaction Path Search. QM-MM restrained energy minimizations have been performed to investigate the reaction path for the conversion of chorismate to prephenate. The distinguished reaction coordinate ξ was taken as the antisymmetric combination of the distances describing the breaking and forming bonds, $\xi = d_{C1-C7} - d_{C3-O1}$, as depicted in Scheme 2. This reaction coordinate has been found to represent very closely the intrinsic reaction coordinate found in the gas phase and in solution.[26,30] For performing the restrained minimizations, an additional term is added to the potential energy. This term is chosen as

$$V_R = \frac{1}{2}k(\xi - \xi_0)^2 \qquad (15)$$

where k is an adjustable force constant, ξ is the value of the reaction coordinate, and ξ_0 is the value of the reaction coordinate for a particular configuration. A value of k of 200 kcal/mol Å^{-2} was found to be adequate. The path is constructed as follows. First, an unrestricted QM-MM minimization is performed for the reactant or product to generate an initial configuration for the reaction path. The reaction path is mapped out by adding the V_R to the potential energy with ξ_0 varying in steps from about −2.0 to 2.0 Å, and performing energy minimizations at each step. The actual energy of each configuration along the reaction path is obtained by subtracting the restraint term from the total energy.

E. Choice of Quantum Subsystem. We have performed QM-MM optimizations and restrained minimizations for two different choices of the quantum subsystem. In the first place, only the substrate was treated quantum mechanically, as shown in Scheme 2. The second choice of the QM subsystem consisted of the substrate moiety plus the charged side chains glu78 and arg90 (Scheme 3). This choice allowed us to consider possible charge transfer to the substrate and polarization effects in these neighbor charged residues, which may be important for the catalytic activity of the enzyme.[28,30] The frontier between the QM and MM portions of the system can be treated by several approaches.[30,42] In our case, the scaled position link atom method (SPLAM)[43] was adapted to our hybrid code. In this method, the bonds between a carbon atom of the QM subsystem (CQM) and a carbon of the MM subsystem (CMM) are replaced with a carbon−hydrogen bond. This hydrogen link atom (Hlink) fills the valence of the QM subsystem, and its position is superimposed on the CQM−CMM bond. Forces exerted on the Hlink are divided in parallel and perpendicular components, the former is added to the CMM and the latter is scaled and summed over CQM and CMM, to avoid including a torque. All classical bond-terms (bonds, angles, and dihedrals) involving at least one CMM central atom are computed normally and are added to the MM potential. Lennard-Jones interactions between the CQM, Hlink, and CMM atoms are omitted for atom pairs separated by less than three bonds. The charge of the CMM atom is divided and summed over its CMM neighbors to maintain the total charge unaltered. This method is efficient and has already been used in previous calculations with different systems including biomolecules.[43,44]

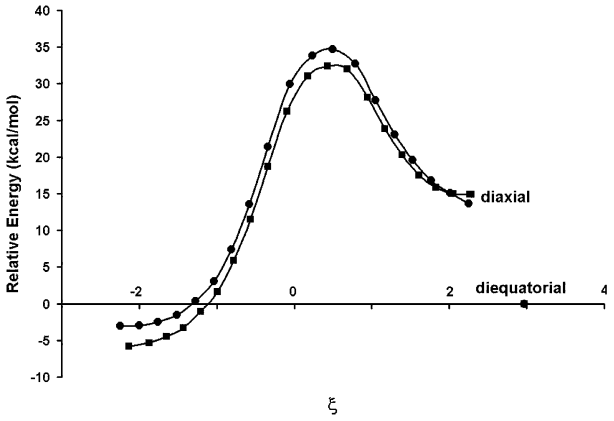

Figure 1. Energy profile for the forward (squares) and inverse (circles) reaction of chorismate to prephenate in vacuum.

Results and Discussion

To validate the SIESTA electronic structure scheme, we have performed geometry optimizations of chorismate and prephenate in vacuum. In Table 1 we report PBE/DZVP results computed with SIESTA for selected optimized geometrical parameters of the reactant (diequatorial conformer) and product, compared with results obtained at the B3LYP/6-31G**[45] level computed with the *Gaussian*98 package[46] (Scheme 2). The computed ΔE of conversion between chorismate and prephenate of −5.8 kcal/mol at the PBE/DZVP level agrees reasonably well with that computed using B3LYP/6-31G** of −4.8 kcal/mol.

Taking into account that the diequatorial to diaxial conformer preequilibrium does not contribute to the total activation free energy of the reaction in aqueous solution and in the enzyme environment,[34] we have computed the energy profile for the conversion of the diaxial chorismate conformer to prephenate. The forward and reverse reactions were examined, and the corresponding energy profiles are shown in Figure 1. We also include the global minimum energy of the reactant, corresponding to the diequatorial conformer. As can be noted in Figure 1, the two profiles agree reasonably well. The computed activation energy in vacuum is 32.4 kcal/mol, in agreement with a previous

TABLE 2: Relevant Energetic Parameters for the Chorismate-to-Prephenate Conversion in Vacuum, Water Solution, and in the Chorismate Mutase Enzyme (kcal/mol)

	ΔE	$\Delta E^{\ddagger}$	$\Delta E^{\ddagger}_{exp}$
vacuum	−5.8	32.4	
aqueous solution	−22.0	13.8	20.7[a]
enzyme (QM subsystem, Scheme 2)	−24.9	5.3	12.7[b]
enzyme (enlarged QM subsystem, Scheme 3)	−30.6	4.3	12.7[b]

[a] Reference 19. [b] Reference 20.

value computed by Houk et al.[21] of 34.3 kcal/mol, at the BLYP/6-31G* level. These values are slightly lower than the reported B3LYP/6-31G* result of 44.0 kcal/mol,[26] consistent with the fact that DFT calculations at the gradient-corrected approximation level usually yield lower activation energies than those obtained using hybrid functionals.[47] The reaction coordinate values are 2.97, 2.25, 0.49, and −2.25 Å for the diequatorial conformer, diaxial conformer, transition state, and product, respectively. Relevant energetic parameters are presented in Table 2.

The computed energy difference between the active diaxial conformer and the most stable diequatorial conformer in vacuum is 14.9 kcal/mol, which compares well with previous calculations of 15.9 kcal/mol[27] and 11.7 kcal/mol,[21] at the MP2/6-31G* and BLYP/6-31G* levels, respectively. This energy difference is mainly due to an intramolecular hydrogen bond between the ring hydroxyl group and the bridged carbonyl group, and is responsible for the very high activation energy for the reaction in gas phase.

The QM-MM calculations in solution were performed by placing the chorismate in a cavity deleted from a 15 Å radius sphere of 664 water molecules. The water molecules were equilibrated by performing 100 ps of classical MD simulations at 200 K, both with chorismate and prephenate as solutes. Geometry optimizations have been performed starting with both reactant and product structures. Only the substrate atoms and the MM atoms lying on a sphere of 11 Å centered on it were allowed to move freely.

The enzyme calculations have been performed employing a starting structure obtained from *B. subtilis* in the Protein Data Bank (1COM).[48] Hydrogen atoms were added as usual. The systems were equilibrated by performing 100 ps of classical MD simulations at 300 K, both with chorismate and prephenate as solutes, to obtain correct starting geometries. We have performed calculations for two different choices of the QM subsystem. In the first case, the full system consisted of a QM region of 24 atoms, (Scheme 2) the substrate molecule, treated at the DFT level, and a MM region, comprising the enzyme plus solvation water molecules (5627 protein atoms plus 1534 TIP3P water molecules). Only the QM atoms and the MM atoms lying on a sphere of 11 Å centered on the QM system were allowed to move freely. The model is depicted in Figure 2. Geometry optimizations have been performed for chorismate and prephenate in the active site. The second choice of the QM subsystem includes the substrate moiety plus the charged side chains glu78 and arg90, as shown in Scheme 3.

The aqueous solution chorismate to prephenate ΔE value of −22.0 kcal/mol compares reasonably well with the results of continuum model calculations of −20.5 kcal/mol,[23] at the B3LYP/6-31G* level. The energy profile is presented in Figure 3. Our computed activation energy is 13.8 kcal/mol, which is lower than the reported experimental value of 20.7 kcal/mol,[19,47] consistent with the computed value in vacuum. The reaction

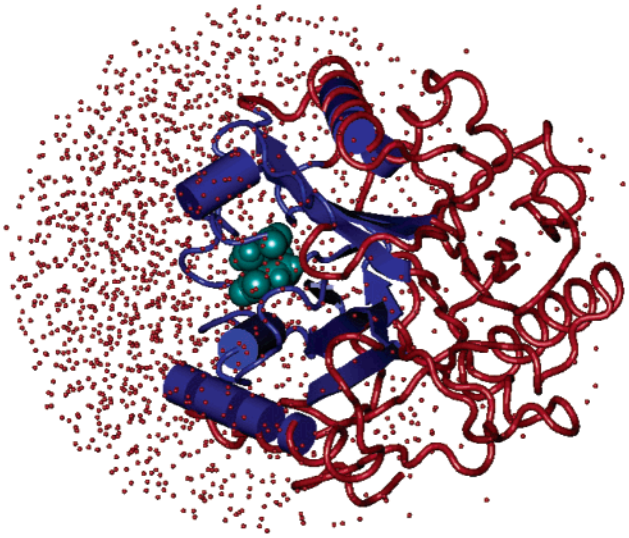

Figure 2. Chorismate mutase model with solvation water molecules (red dots). The substrate is depicted in cyan, the MM free atoms are depicted in blue, whereas the frozen ones are depicted in red.

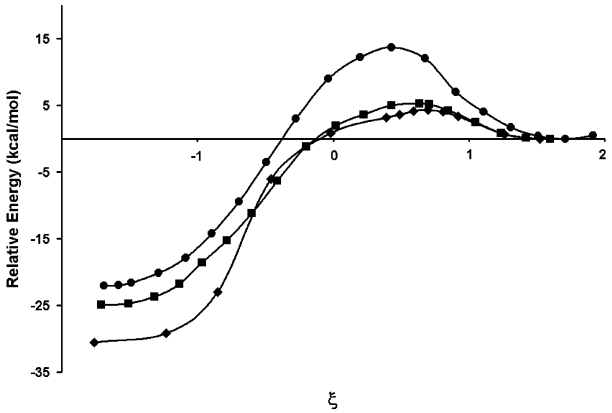

Figure 3. Energy profile for the reaction of chorismate to prephenate in aqueous solution (circles) and in the enzyme with the two different QM subsystems: substrate (squares), substrate plus the charged side chains glu78 and arg90 (rombus).

coordinate values are 1.71, 0.43, and −1.69 Å for the reactant, transition state, and product, respectively. Relevant energetic parameters are presented in Table 2.

For the smaller QM subsystem, our predicted chorismate to prephenate ΔE in the enzyme is −24.9 kcal/mol. This lower result with respect to solution could be explained by considering that when the rearrangement is taking place an additional hydrogen bond between arg90(HH11) and glu78(OE1) is formed. This hydrogen bond is formed only for values of the reaction coordinate lower than about −0.8 Å, and consequently, it is only present in the product. This additional interaction is responsible for the more negative chorismate-to-prephenate ΔE value for the reaction in the presence of the enzyme (−24.9 kcal/mol) compared to the computed value in water (−22.0 kcal/mol) (Table 2 and Scheme 4). It is important to note that the requirement for ΔE (reactant−product) to be the same in solution and in the enzyme-catalyzed reaction is valid only when both the initial and final states have the reactant and product unbound from the enzyme. It is then not surprising that we obtain different equilibrium ΔE in solution and inside chorismate mutase. The enzymatic energy profile is also presented in Figure 3. The reaction coordinate values are 1.60 Å, 0.71 Å and −1.71 Å for the reactant, transition state and product, respectively. Energetic results are also presented in Table 2. It is clear that

SCHEME 4. Active Site Model of *B. subtilis* Chorismate Mutase Enzyme

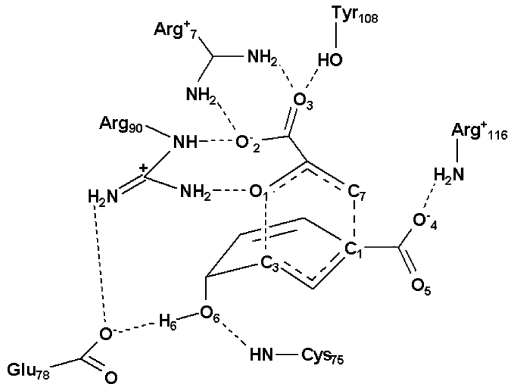

our results reproduce the catalytic effect of the enzyme, since the computed activation energy reduces from 13.8 kcal/mol to 5.3 kcal/mol when going from aqueous solution to the enzyme. The computed activation energy is lower than the reported experimental value of 12.7 kcal/mol,[20,47] but the computed difference between the activation energies of the reaction in water and in the enzyme, $\Delta(\Delta E^{\ddagger})$ of 8.5 kcal/mol, agrees very well with the experimental value of 8 kcal/mol. The predicted activation energy value is in the typical range of activation energies for enzymatic reactions (about 5−10 kcal/mol).

To analyze the different contributions to the activation energy, we have carried out an analysis of the different energy terms of chorismate and transition state optimized structures, as suggested by Marti et al.[26] The total QM-MM activation energies obtained in aqueous solution or in the enzyme environment can be written as the following sum:

$$\Delta E^{\ddagger} = \Delta E_{QM} + \Delta E_{MM} + \Delta E_{int} \qquad (16)$$

where each contribution corresponds to single point energy calculations of the transition state, relative to the reactant, computed at the structures obtained in the QM-MM calculations. The terms ΔE_{QM}, ΔE_{MM}, and ΔE_{int}, correspond to the in vacuo DFT energy, the MM contribution, and the substrate−environment interaction energy, respectively. The ΔE_{QM} values are 13.5 and 11.5 kcal/mol for water and enzyme, respectively. The transition state relative energy is slightly (2 kcal/mol) more favorable in the enzyme active site than in water. This steric contribution to the activation energy in the enzyme is attributed to a more compressed reactant structure than in solution. This is also reflected in the fact that the reaction coordinate value corresponding to chorismate in solution is 1.71 Å, whereas in the enzyme is 1.60 Å.

We can also compare the E_{QM} single point QM energies of the substrate at the optimized structures in aqueous solution and protein. The difference in chorismate E_{QM} values between solution and protein shows that the substrate is destabilized by steric compression in 2.1 kcal/mol. This effect has been reported by Jorgensen et al.[34] to be of about 9 kcal/mol. This magnitude computed for the transition state is only 0.1 kcal/mol. These facts reflect that the steric compression of the reactant by the enzyme destabilizes it and hence reduces the activation energy.

Steric compression effects have also been analyzed by Khanjin et al.[25] by performing DFT calculations on a set of chorismate conformationally restricted analogues in vacuum. Our chorismate optimized C1−C7 bond distances are 4.42, 3.62, and 3.13 Å, in vacuum, water, and protein, respectively. On the other hand, the optimized C1−C7 distances in the TS span a much smaller window, with 2.61, 2.53, and 2.64 Å, in vacuum, water, and protein, respectively. Following these authors' analysis, this confirms that steric compression effects are more important in the reactant than in the TS.

TABLE 3: Relevant Geometrical Parameters of Chorismate, Transition States, and Prephenate Complexed with the Enzyme (Å)

	chorismate	transition state	prephenate
C1−C7	3.13	2.64	1.59
C3−O1	1.53	1.93	3.30
H6−glu78(OE1)	1.49	1.46	1.54
O1−arg90(HH22)	1.80	1.74	1.90
O2−arg90(HE)	1.80	1.83	1.81
O2−arg7(HH21)	1.80	1.79	1.77
O3−arg7(HH12)	1.88	1.90	1.86
O3−tyr108(HH)	1.76	1.75	1.75
O4−arg116(HH12)	1.87	1.86	1.87
O6−cys75(H)	1.99	1.96	1.91
arg90(HH11)−glu78(OE1)	3.69	3.64	1.85

The ΔE_{int} values of 5.9 kcal/mol for water and −4.7 kcal/mol in the enzyme show that the major catalytic character of the enzyme comes from an important stabilization of the transition state due to a favorable electrostatic enzyme−transition state interaction. This effect is not observed in water, where the substrate is more stabilized. The electrostatic stabilization of the transition state by the enzyme is about 10.6 kcal/mol, with respect to water. The ΔE_{MM} values are −5.6 kcal/mol and −1.5 kcal/mol for water and enzyme, respectively. In both cases, the environment rearrangement stabilizes preferentially the transition state. In solution, this negative value almost compensates the unfavorable ΔE_{int}, resulting in a net activation energy of approximately 13 kcal/mol. The rearrangement energy in the enzyme is not an important contribution to the activation energy. Taking all these contributions into account, we can conclude that the catalytic activity achieved by the enzyme in comparison with the aqueous solution reaction is mainly due to both a major electrostatic stabilization of the transition state by the enzyme and a minor steric compression and hence destabilization of the substrate.

Relevant geometrical parameters are shown in Table 3 (Scheme 4) for the enzyme complexed with chorismate, transition state, and prephenate. It can be seen that the enzyme locks them in its active site by making strong contacts with the relevant nearest residues. The strongest interactions are shown to be with residues glu78, arg90, arg7, tyr108, arg116, and cys75. It is important to remark that most distances between the substrate and these residues do not change significantly during the rearrangement. However, as can be seen from Table 3, H6-glu78(OE1) and O1-arg90(HH22) hydrogen bond distances are the ones that get shorter (from 1.49 and 1.80 Å to 1.46 and 1.74 Å, respectively) when going from the reactant to the transition state, consistently with its preferential electrostatic stabilization. Moreover, these two distances are longer in the product structures than in both reactant and transition state (1.49 and 1.80 Å in reactant and 1.54 and 1.90 Å in product, respectively). This hydrogen bond weakening is related to the formation of an additional arg90(HH11)−glu78(OE1) hydrogen bond, which is present only in the product structure, as can be noted by comparing the arg90(HH11)−glu78(OE1) distances of 3.69 and 1.85 Å in reactant and product, respectively.

The simulations performed with the second choice of the QM subsystem, including the substrate plus the charged side chains glu78 and arg90, yield a chorismate-to-prephenate ΔE value of −30.6 kcal/mol, compared with −24.9 kcal/mol for the smaller QM subsystem. This is probably due to the fact that the

TABLE 4: Mulliken Charges of Relevant Atoms and Groups Complexed with the Enzyme

	QM subsystem (Scheme 2)			enlarged QM subsystem (Scheme 3)		
	chorismate	TS	prephenate	chorismate	TS	prephenate
O1	−0.274	−0.372	−0.250	−0.228	−0.292	−0.148
C3	0.236	0.330	0.184	0.276	0.332	0.198
C1	0.158	0.190	0.256	0.160	0.196	0.258
C7	0.370	0.398	0.366	0.370	0.380	0.360
O6	−0.176	−0.172	−0.148	−0.156	−0.160	−0.120
H6	0.052	0.062	0.028	−0.126	−0.128	−0.102
glu78	−1.0	−1.0	−1.0	−0.67	−0.63	−0.48
arg90	1.0	1.0	1.0	0.66	0.62	0.44
substrate	−2.0	−2.0	−2.0	−1.99	−1.99	−1.96

hydrogen bond between arg90(HH11) and glu78(OE1) is stronger when these residues are treated quantum mechanically. The energy profile for these calculations is presented in Figure 3, and energetic results are also presented in Table 2. The computed activation energy is 4.3 kcal/mol, which is slightly lower than the previous value of 5.3 kcal/mol predicted for the smaller QM subsystem.

A significant degree of charge transfer is observed between arg90 and O1, as can be seen by comparing the O1 Mulliken populations for the two choices of QM subsystem. The same effect is noted for the Mulliken populations of H6 and O6, due to charge transfer from glu78 (Table 4). This is consistent with previous results obtained by Lee et al.[30] Strong charge transfer effects between arg90 and glu78 are also observed, especially for the product structure where a hydrogen bond between them is present. For both QM subsystems, C3 and O1 Mulliken charges increase when going from reactant to transition state, consistent with the preferential electrostatic stabilization of the transition state. The smaller values for these charges in the product with respect to both reactant and transition state are probably related to the weakening of the hydrogen bonds with arg90(HH22) and glu78(OE1), due to the formation of the hydrogen bond between arg90(HH11) and glu78(OE1). Both charge transfer and polarization effects between the substrate and the residues arg90 and glu78 are operative when these residues are included in the QM subsystem. On the other hand, only polarization effects by the neighbor amino acids are considered when using the substrate as the QM subsystem. However, the activation energy computed with both choices of the QM charge subsystem is similar, suggesting that the catalytic activity of the enzyme is mainly related to substrate polarization effects.

Conclusions

We have successfully presented a hybrid QM-MM implementation that includes a description of the QM system at the DFT level, as implemented in the computationally efficient program SIESTA. We have applied this QM-MM scheme to the conversion of chorismate to prephenate in aqueous solution and in the active site of *B. subtilis* chorismate mutase enzyme. We have predicted a catalytic activity in the enzyme environment with respect to the uncatalyzed solution reaction, reflected in an activation energy difference $\Delta(\Delta E^{\ddagger})$ of 8.5 kcal/mol ($k_{cat}/k_{uncat} = 1.56 \times 10^6$). This value agrees very well with the experimental value of 8 kcal/mol ($k_{cat}/k_{uncat} = 6.73 \times 10^5$). The catalytic activity achieved by the enzyme in comparison with the aqueous solution reaction is mainly due to both a major electrostatic stabilization of the transition state by the enzyme and a minor steric compression and hence destabilization of the substrate, reducing the activation energy of the reaction.

Acknowledgment. This work was partially supported by grants from Fundación Antorchas, Universidad de Buenos Aires, and ANPCYT. We thank Pablo de Grande, Microsoft Argentina, and the LBP Endowment for the Sciences and Arts for a generous donation. D.A.E. is member of the scientific staff of CONICET. P.O acknowledges support from Spain Fundación Ramón Areces and MCyT. A.C. acknowledges the simus for their help and A.R.G. This work was partially supported by National Computational Science Alliance to A.E.R.

References and Notes

(1) Scuseria, G. E. *J. Phys. Chem. A* **1999**, *103*, 4782.
(2) Gogonea, V.; Merz, K. M., Jr. *J. Phys. Chem. A* **1999**, *103*, 5171.
(3) Greatbanks, S. P.; Gready, J. E.; Limaye, A. C.; Rendell, A. P. *J. Comput. Chem.* **2000**, *21*, 788.
(4) York, D.; Lee, T.; Yang, W. *Phys. Rev. Lett.* **1998**, *80*, 5011.
(5) Lewis, J. P.; Carter, C. W., Jr.; Hermans, J.; Pan, W.; Lee, T.; Yang, W. *J. Am. Chem. Soc.* **1998**, *120*, 5407.
(6) Khandogin, J.; York, D. M. *J. Phys. Chem. B* **2002**, *106*, 7693.
(7) Merz, K. M., Jr. *Encycl. Comput. Chem.* **1998**, *4*, 2330.
(8) Monard, G.; Merz, K. M., Jr. *Acc. Chem. Res.* **1999**, *32*, 904.
(9) Walker, R. C.; de Souza, M. M.; Mercer, I. P.; Gould, I. R.; Klug, D. R. *J. Phys. Chem. B* **2002**, *106*, 11658.
(10) Bruice, T. C. *Acc. Chem. Res.* **2002**, *35*, 139.
(11) Orozco, M.; Luque, F. J. *Chem. Rev.* **2000**, *100*, 4187.
(12) Kohanoff, J.; Koval, S.; Estrin, D. A.; Laria, D.; Abaskin, Y. *J. Chem. Phys.* **2000**, *112*, 9498.
(13) Elola, M. D.; Laria, D.; Estrin, D. A. *J. Phys. Chem. A* **1999**, *103*, 5105.
(14) Soler, J. M.; Artacho, E.; Gale, J. D.; García, A.; Junquera, J.; Ordejón, P.; Sánchez-Portal, D. *J. Phys.: Condens. Matter* **2002**, *14*, 2745.
(15) Reich, S.; Thomsen, C.; Ordejón, P. *Phys. Rev. B* **2002**, *65*, 155411.
(16) Wang, J.; Cieplak, P.; Kollman, P. A. *J. Comput. Chem.* **2000**, *21*, 1049.
(17) Bartlett, P. A.; Nakagawa, Y.; Johnson, C. R.; Reich, S. H.; Luis, A. J. *J. Org. Chem.* **1988**, *53*, 3195.
(18) Haslam, E. *Shikimic Acid: Metabolism and Metabolites*; John Wiley & Sons: New York, 1993.
(19) Andrews, P. R.; Smith, G. D.; Young, I. G. *Biochemistry* **1973**, *18*, 3492.
(20) Galopin, C. C.; Zhang, S.; Wilson, D. B.; Ganem, B. *Tetrahedron Lett.* **1996**, *37*, 8675.
(21) Wiest, O.; Houk, K. N. *J. Am. Chem. Soc.* **1995**, *117*, 11628.
(22) Wiest, O.; Montiel, D. C.; Houk, K. N. *J. Phys. Chem. A* **1997**, *101*, 8378.
(23) Kast, P.; Tewari, Y. B.; Wiest, O.; Hilvert, D.; Houk, K. N.; Goldberg, R. N. *J. Phys. Chem. B* **1997**, *101*, 10976.
(24) Davidson, M. M.; Guest, J. M.; Craw, J. S.; Hillier, I. H.; Vincent, M. A. *J. Chem. Soc., Perkin Trans. 2* **1997**, 1395.
(25) Khanjin, N. A.; Snyder, J. P.; Menger, F. M. *J. Am. Chem. Soc.* **1999**, *121*, 11831.
(26) Martí,, S.; Andrés, J.; Moliner, V.; Silla, E.; Tuñon, I.; Bertrán, J.; Field, M. J. *J. Am. Chem. Soc.* **2001**, *123*, 1709.
(27) Martí, S.; Andrés, J.; Moliner, V.; Silla, E.; Tuñon, I.; Bertrán, J. *J. Phys. Chem. B* **2000**, *104*, 11308.
(28) Worthington, S. E.; Roitberg, A. E.; Krauss, M. *J. Phys. Chem. B* **2001**, *103*, 7087.
(29) Roitberg, A. E.; Worthington, S. E.; Holden, M. J.; Mayhew, M. P.; Krauss, M. *J. Am. Chem. Soc.* **2000**, *122*, 7312.
(30) Lee, Y. S.; Worthington, S. E.; Krauss, M.; Brooks, B. R. *J. Phys. Chem. B* **2002**, *106*, 12059.
(31) Woodcock, H. L.; Hodoscek, M.; Sherwood, P.; Lee, Y. S.; Schaefer, H. F., III; Brooks, B. R. *Theor. Chem. Acc.* **2003**, *109*, 140.

(32) Carlson, H. A.; Jorgensen, W. L. *J. Am. Chem. Soc.* **1996**, *118*, 8475.

(33) Repasky, M. P.; Guimarães, C. R. W.; Chandrasekhar, J.; Tirado-Rives, J.; Jorgensen, W. L. *J. Am. Chem. Soc.* **2003**, *125*, 6663.

(34) Guimarães, C. R. W.; Repasky, M. P.; Chandrasekhar, J.; Tirado-Rives, J.; Jorgensen, W. L. *J. Am. Chem. Soc.* **2003**, *125*, 6892.

(35) Gou, H.; Cui, Q.; Lipscomb, W. N.; Karplus, M. *Biochemistry* **2001**, *98*, 9032.

(36) Sánchez-Portal, D.; Ordejón, P.; Artacho, E.; Soler, J. M. *Int. J. Quantum Chem.* **1997**, *65*, 453.

(37) Artacho, E.; Sánchez-Portal, D.; Ordejón, P.; García, A.; Soler, J. M. *Phys. Status Solidi B* **1999**, *215*, 809.

(38) Sankey, O. F.; Niklewski, D. J. *Phys. Rev. B* **1989**, *40*, 3979.

(39) Kleinman, L.; Bylander, D. M. *Phys. Rev. Lett.***1982**, *48*, 1425.

(40) Perdew, J. P.; Burke, K.; Ernzerhof, M. *Phys. Rev. Lett.* **1996**, *77*, 3865.

(41) Jorgensen, W. L. *J. Am. Chem. Soc.* **1981**, *103*, 335.

(42) Reuter, N.; Dejaegere, A.; Maigret, B.; Karplus, M. *J. Phys. Chem. A* **2002**, *104*, 1720.

(43) Eichinger, M.; Tavan, P.; Hutter, J.; Parrinello, M. *J. Chem. Phys.* **1999**, *110*, 10452.

(44) Rovira, C.; Schultze, B.; Eichinger, M.; Evanseck, J. D.; Parrinello, M. J. *Biophys. J.* **2001**, *81*, 435.

(45) (a) Becke, A. *J. Chem. Phys.* **1993**, *98*, 5648. (b) Lee, C.; Yang, W.; Parr, R. *Phys. Rev. B* **1988**, *37*, 785.

(46) Frisch, M. J.; Trucks, G. W.; Schlegel, H. B.; Scuseria, G. E.; Robb, M. A.; Cheeseman, J. R.; Zakrzewski, V. G.; Montgomery, J. A., Jr.; Stratmann, R.; Burant, J.; Dapprich, S.; Millam, J. M.; Daniels, A. D.; Kudin, K. N.; Strain, M. C.; Farkas, O.; Tomasi, J.; Barone, V.; Cossi, M.; Cammi, R.; Mennucci, B.; Pomelli, C.; Adamo, C.; Clifford, S.; Ochterski, J.; Petersson, G. A.; Ayala, P. Y.; Cui, Q.; Morokuma, K.; Malick, D. K.; Rabuck, A. D.; Raghavachari, K.; Foresman, J. B.; Cioslowski, J.; Ortiz, J. V.; Baboul, A. G.; Stefanov, B. B.; Liu, G.; Liashenko, A.; Piskorz, P.; Komaromi, I.; Gomperts, R.; Martin, R. L.; Fox, D. J.; Keith, T.; Al-Laham, M. A.; Peng, C. Y.; Nanayakkara, A.; Gonzalez, C.; Challacombe, M.; Gill, P. M. W.; Johnson, B.; Chen, W.; Wong, M. W.; Andres, J. L.; Gonzalez, C.; Head-Gordon, M.; Replogle, E. S.; Pople, J. A. *Gaussian 98*, Rev. A7, Gaussian, Inc.: Pittsburgh, PA, 1998.

(47) Baker, J.; Muir, M.; Andzelm, J. *J. Chem. Phys.* **1995**, *102*, 2063.

(48) Chook, Y. M.; Gray, J. V.; Ke, H.; Lipscomb, W. N. *J. Mol. Biol.* **1994**, *240*, 476.